# Electroproduction of medium- and heavy-mass hypernuclei

P. Bydžovský<sup>1</sup>, D. Denisova<sup>1</sup>, F. Knapp<sup>2</sup>, and P. Veselý<sup>1</sup>

<sup>1</sup>Nuclear Physics Institute, ASCR, 25068 Řež/Prague, Czech Republic

<sup>2</sup>Institute of Particle and Nuclear Physics, Faculty of Mathematics and Physics, Charles University, V Holešovičkách 2, 18000 Prague, Czech Republic

(Dated: March 7, 2025)

The DWIA formalism for computing the cross sections in electroproduction of hypernuclei used before for lighter (p-shell and sd-shell) systems is utilized in studying electroproduction on heavier targets such as  $^{52}{\rm Cr}$ , and  $^{208}{\rm Pb}$ . First, the effects from kaon distortion and kinematics are reexamined and then results for the heavy targets are discussed in view of various forms of the  $\Lambda N$  effective interaction, the elementary amplitude, and kinematics. Apparent sensitivity of the hypernucleus excitation spectra to various forms of the  $\Lambda N$  effective interaction is shown. Predictions of the excitation spectrum in electroproduction of  $^{208}{}_{\Lambda}{\rm Tl}$  are also given in kinematics of the experiment E12-20-013 in preparation at Jefferson Lab.

### I. INTRODUCTION

Investigation of hypernucleus properties provides significant information about the baryon-baryon interaction with a non zero strangeness. Processes involving production of hypernuclei play important role as they allow to study effective forms of the interaction. The measured excitation spectra and cross sections give information about details of the interaction. To this end, one should have a good understanding of the reaction mechanism to be able to draw firm conclusions from a data analysis.

The hypernuclei have been already studied for several decades in various reactions [1, 2]. ity of obtained data depends on the reaction where the best precision was achieved in the measurement of  $(\pi^+, K^+\gamma)$  [2]. These high-quality  $\gamma$ -ray data for pshell hypernuclei allowed performing a detailed analysis of the spin-dependent part of the effective hyperonnucleon (YNG) interaction [3]. The hypernuclei were also studied in the  $(\pi^+, K^+)$  reaction [2, 4] providing mainly information about the binding energies of  $\Lambda$  in various shells and the cross sections for production of the ground state. Reaction spectra with a better energy resolution than in  $(\pi^+, K^+)$  were obtained from the  $(e, e'K^+)$  reaction measured for the first time at Jefferson Lab [5]. Data from the successive measurements of electroproduction of p-shell hypernuclei performed at Jefferson Lab then allowed studying the YNG interaction [6]. Heavier hypernuclei beyond the p-shell were investigated in the past utilizing mainly the  $(\pi^+, K^+)$  reaction [4]. However, new experiments for electroproduction of hypernuclei on the medium-mass,  $^{40}$ Ca and  $^{48}$ Ca (E12-15-008 [7]), and heavy, <sup>208</sup>Pb (E12-20-013 [8]), targets are planned at Jefferson Lab.

Electroproduction of  $\Lambda$  hypernuclei provides not only a test ground for various effective YNG interactions but it also allows studying the reaction mechanism and the elementary amplitudes at very small kaon angles. The theoretical photoproduction excitation spectra obtained in the distorted-wave impulse approximation (DWIA) for the p-shell and medium-mass hypernuclei were discussed

by Motoba et.al. in Refs. [9] and [10]. It was shown that the spectra for typical medium-mass hypernuclei such as  $^{28}_{\Lambda}$ Al and  $^{40}_{\Lambda}$ K provide interesting opportunities of spectroscopic study beyond the p shell. Another analysis of the cross sections in photoproduction of light  $\binom{12}{\Lambda}$ B) as well as very heavy  $\binom{208}{\Lambda}$ Tl) hypernuclei was performed in Ref. [11] showing the wide applicability of the  $(e, e'K^+)$ reaction. In our previous analysis [12–14] of hypernucleus electroproduction we studied the kinematical and Fermi motion effects in the case of p-shell hypernuclei  $(^{12}_{~\Lambda}\rm B,~^{16}_{~\Lambda}N,~^{9}_{\Lambda}\rm Li)$  [13] and verified that the nucleus and hypernucleus structure of medium-mass systems ( $^{28}_{~\Lambda}\rm Al,$ <sup>40</sup>K) can be realistically described in the Tamm-Dancoff approach [14]. Here we continue our study focusing on the medium- and heavy-mass hypernuclei and providing predictions for the experiments E12-15-008 and E12-20-013.

The paper is organized as follows: in Section II we give a brief overview of basic formalism. More details can be found in Refs. [13] and [14]. In Section III, the effects from kaon distortion, kinematics, and Fermi motion are discussed in the case of heavy hypernuclei. Here we also elaborate the optimum on-shell approximation introduced in Ref. [13]. The excitation spectra in electroproduction of medium- and heavy-mass hypernuclei,  $^{40}_{\Lambda} \mathrm{K}, \, ^{48}_{\Lambda} \mathrm{K}, \, ^{52}_{\Lambda} \mathrm{V},$  and  $^{208}_{\Lambda} \mathrm{Tl},$  are discussed in Sec. IV. The summary and conclusions from our study are given in Sec. V.

## II. BASIC FORMALISM

The cross section in electroproduction of hypernuclei is calculated in the impulse approximation (IA) considering the optimal factorization approximation where the amplitude for elementary production is evaluated for an effective proton momentum [13]. The general form of the two-component elementary amplitude, constructed in Ref. [13], allows for an arbitrary value of this momentum. In the previous analysis we had suggested an optimum value of the effective proton momentum which fulfills the necessary kinematical conditions and the elementary am-

plitude is on-shell. In the many-particle matrix element, the photon plane wave and kaon distorted wave are decomposed into partial waves (LM) and the target proton and final  $\Lambda$  are supposed to occupy the single-particle states  $\alpha \ (=n,l,j)$  and  $\alpha'$ , respectively. The reduced amplitude, used to compute the cross sections, then reads

$$A_{Jm}^{\lambda} = \frac{1}{[J]} \sum_{S\eta} \mathcal{F}_{\lambda\eta}^{S} \sum_{LM} C_{LMS\eta}^{Jm} \sum_{\alpha'\alpha} \mathcal{R}_{\alpha'\alpha}^{LM} \mathcal{H}_{l'j'lj}^{LSJ} \times (\Phi_{H} || [b_{\alpha'}^{+} \otimes a_{\alpha}]^{J} || \Phi_{A}), \qquad (1)$$

where  $\mathcal{F}_{\lambda\eta}^S$  are spherical elementary amplitudes with a baryon spin-flip S=0,1 and photon helicity  $\lambda=\pm 1,0$ . The nucleus( $\Phi_A$ )-hypernucleus( $\Phi_H$ ) transition is described by the radial integral  $\mathcal{R}_{\alpha'\alpha}^{LM}$  and the one-body density matrix element (OBDME), where  $a_{\alpha}$  and  $b_{\alpha'}^+$  are the proton annihilation and  $\Lambda$  particle creation operators. The term  $\mathcal{H}_{l'j'lj}^{LSJ}$  includes the Racah algebra and  $C_{LMS\eta}^{Jm}$  is the Clebsch-Gordan coefficient. Derivation of this formula and expressions for the cross sections can be found in Ref. [13].

The radial integrals are explicitly

$$\mathcal{R}_{\alpha'\alpha}^{LM} = \int_0^\infty d\xi \, \xi^2 \, R_{\alpha'}(\xi)^* \, F_{LM}(\Delta B \xi) \, R_{\alpha}(\xi) \,, \quad (2)$$

where  $R_{\alpha'}$  and  $R_{\alpha}$  are the  $\Lambda$  and proton radial wave functions, respectively, and  $F_{LM}$  comes from the partial-wave decomposition of the photon and kaon waves, see appendix C in Ref. [13]. This function depends on the momentum transfer  $\Delta = |\vec{P_{\gamma}} - \vec{P_{K}}|$  and parameter  $B = (A-1)/(A-1+m_{\Lambda}/m_{p})$ . Note that in the case without a kaon distortion in PWIA the function  $F_{LM}$  corresponds to the spherical Bessel function.

Kaon distortion is in our approach included by means of the eikonal approximation with the first-order optical potential. The kaon distorted wave then reads as [15]

$$\chi_{\rm K}^+(\vec{r}\,) = \exp\left[-b\,\sigma_{\rm KN}^{tot}(s)\Big(1-i\alpha(s)\Big)\!\!\int_0^\infty\!\!\!dt\,\rho(\vec{r}+\hat{p}\,t)\right], \eqno(3)$$

where  $\sigma_{\text{KN}}^{tot}$  is the kaon-nucleon (KN) total cross section and  $\alpha(s) = \text{Re} f_{\text{KN}}(s,0)/\text{Im} f_{\text{KN}}(s,0)$ , with the KN amplitude at zero angle and invariant energy squared s. The parameter b stands for a kinematical factor [15] and the integrand  $\rho(\vec{r} + \hat{p}t)$  describes the nucleon density where  $\hat{p}$  is a unit vector in direction of the relative kaon-hypernucleus momentum.

The nucleus and hypernucleus structure included in OBDME, ( $\Phi_H || [b_{\alpha'}^+ \otimes a_{\alpha}]^J || \Phi_A$ ), and the radial single-particle wave functions  $R_{\alpha}$  are calculated using a many-particle formalism with specific NN and YN effective interactions. In the present analysis we use the Hartree-Fock (HF) and Tamm-Dancoff (TD<sub>\Lambda</sub>) approaches [14, 16]. In Refs. [14, 16] the HF was solved for hypernuclear Hamiltonian which included two-body  $(NN, N\Lambda)$ , and three-body (NNN) interactions. In this paper we do not include the three-body NNN interaction term. Instead,

to mimic the many-nucleon interactions in the nuclear Hamiltonian, we complement the NN interaction with a phenomenological density-dependent (DD) term [17]

$$v_{\rho} = \frac{C_{\rho}}{6} (1 + P_{\sigma}) \rho \left( \frac{\vec{r}_1 + \vec{r}_2}{2} \right) \delta(\vec{r}_1 - \vec{r}_2),$$
 (4)

where  $C_{\rho}$  is a coupling constant which plays role of a free parameter,  $P_{\sigma}$  is the operator of the spin exchange, and  $\rho$  is the nucleon density of the calculated nucleus.

Applying the HF method for description of  $^{40}$ Ca,  $^{48}$ Ca,  $^{52}$ Cr, and  $^{208}$ Pb we obtain the proton and neutron single-particle states. The  $\Lambda$  single-particle states are obtained by solving the additional Schrödinger-like equation (see Eq. (4) in [16]). In the case of  $^{52}$ Cr, which consists of 24 protons and 28 neutrons, we solve the HF equations by using the approximation of partial occupation of the proton valence  $0f_{7/2}$  level by 4 instead of 8 protons.

The hypernuclei  ${}^{40}_{\Lambda}$ K,  ${}^{48}_{\Lambda}$ K,  ${}^{52}_{\Lambda}$ V, and  ${}^{208}_{\Lambda}$ Tl are described within TD<sub> $\Lambda$ </sub> approach [14, 16] in which we diagonalize the hypernuclear Hamiltonian in the space of  $\Lambda$ -particle proton-hole excitations on top of the HF states of  ${}^{40}$ Ca,  ${}^{48}$ Ca,  ${}^{52}$ Cr, and  ${}^{208}$ Pb, respectively.

The HF + TD<sub> $\Lambda$ </sub> calculations are performed within a harmonic oscillator (HO) basis, which should be large enough in order to reach the convergence with respect to a HO frequency. It is sufficient to use the space up to  $N_{\rm max}=12$  major shell.

The nucleon-nucleon interaction is described by the Daejeon 16 [18, 19] NN interaction complemented with the phenomenological DD term (4) which we denote as D16+DDT. The Daejeon 16 interaction itself is derived from the NN component of chiral N3LO potential [20]. subsequently softened by a SRG transformation [21] with flow parameter  $\lambda = 1.5 \text{ fm}^{-1}$ . The phenomenological DD term mimic the effects of the 3-body and higher-body nucleon interactions and its coupling constant  $C_{\rho}$  was tuned for each nucleus separately in order to obtain a realistic description of nuclear radii and nucleon single-particle energies. The  $N\Lambda$  interaction is described using various effective G-matrix potentials based on the YN interactions Nijmegen F [22], Jülich A [22], and chiral LO [23]. The G-matrix derived from the Nijmegen F, and Jülich A interactions is parametrized as a sum of Gaussian-like terms

$$V_{\Lambda N} = \sum_{i=1}^{3} (a_i + b_i k_{\rm F} + c_i k_{\rm F}^2) \exp(-r^2/\beta_{\rm i}^2), \quad (5)$$

which depend on the Fermi momentum  $k_F$ . The coefficients  $a_i$ ,  $b_i$ ,  $c_i$ , and  $\beta_i$  are given in Ref. [22]. The interaction matrix elements of the G-matrix derived from the chiral LO YN potential [23]  $G_{ijkl}(\Omega) = \langle ij|\hat{G}(\Omega)|kl\rangle$  are obtained by solving a first approximation of the Bethe-Goldstone equation

$$G_{ijkl}(\Omega) = V_{ijkl}^{N\Lambda - N\Lambda}$$

$$- \sum_{mn} V_{ijmn}^{N\Lambda - N\Sigma} \frac{1}{(\epsilon_m^N + \epsilon_n^{\Sigma}) - \Omega} V_{klmn}^{N\Lambda - N\Sigma},$$
(6)

where  $\Omega$  is a parameter of the G-matrix,  $V^{N\Lambda-N\Lambda}$  ( $V^{N\Lambda-N\Sigma}$ ) is the  $N\Lambda-N\Lambda$  ( $N\Lambda-N\Sigma$ ) channel of the LO YN interaction, and  $\epsilon_m^N$  ( $\epsilon_m^\Sigma$ ) are nucleon ( $\Sigma$ ) single-particle energies. The sum over single-particle states in Eq. (6) runs only over unoccupied nucleon states. The single-particle energies  $\epsilon_m^\Sigma$  were obtained by using the  $N\Sigma-N\Sigma$  channel of the LO YN interaction in the equation analogous to that which we solve to obtain the single-particle levels of  $\Lambda$  (see Eq. (4) in [16]). The parameter  $\Omega$  in Eq. (6) is defined as

$$\Omega = E_{\rm av} - (m_{\Sigma^0} - m_p), \qquad (7)$$

where  $m_{\Sigma^0}$   $(m_p)$  is mass of  $\Sigma^0$  (proton), respectively, and  $E_{\rm av}$  is either a free parameter or we can determine it as an average energy of occupied nucleons, i.e.  $E_{\rm av} = \sum_i \epsilon_i^N v_i / \Lambda$ , where the coefficient  $v_i = 1$  for the occupied single-particle states, and  $v_i = 0$  otherwise.

# III. EFFECTS FROM KAON DISTORTION AND KINEMATICS

Before we will show results for the heavy hypernuclei we discuss in more detail effects from re-scattering of kaons in the final state and from shifting the hypernucleus mass due to an excitation energy. The latter was used in our approach [6, 13, 14] but has not been discussed yet.

As shown in Eq. (3) the kaon distorted wave depends on the nucleon density and kaon-nucleon (KN) scattering amplitude. For the latter we utilize a separable form constructed in Ref. [24]. This form was also used in description of kaon scattering on nuclei [25, 26]. Here and in the previous hypernucleus DWIA calculations [6, 12] we have utilized an improved version of the separable KNamplitude which includes the partial waves up to l=7and which can describe the available KN data up to the invariant energy of about 2.4 GeV. This is especially important for the hypernucleus calculations at photon energies of about 2 GeV [6] as other KN amplitudes, e.g. that in Ref [27], fail to describe the KN scattering at those energies. Note also that this new separable KNamplitude is isospin dependent and therefore the distortion differs for various targets according to a number of the protons and neutrons, e.g. in <sup>40</sup>Ca and <sup>48</sup>Ca.

The nucleon density  $\rho$  in Eq. (3) is described by the Hartree-Fock (HF) form which is taken from the HF many-particle calculations consistently with OB-DME. However, in our previous calculations for the p-shell hypernuclei [6, 12–14] we used a phenomenological parametrization motivated by the harmonic oscilator model (HO) [15]

$$\rho_{\text{HO}}(r) = (a_0 + a_1 \alpha^2 r^2) \exp(-\alpha^2 r^2)$$
 (8)

with the parameters  $a_0$ ,  $a_1$  and  $\alpha$  depending on the nucleus mass number A and the HO parameter  $b_{\rm HO}$  [15]. In next discussion we compare influence of the HF and

HO forms of the nucleon density on the cross sections. Remind that in our approach the kaon distortion is included via the eikonal approximation with the first-order kaon-nucleus optical potential.

In the case of light p-shell hypernuclei like  $^{12}_{\Lambda}$ B the electroproduction cross section is decreased due to the kaon final-state re-scattering by 45% for the ground-state doublet with  $\Lambda$  in the s orbit and by 34% for the multiplet at about 11 MeV with  $\Lambda$  in the p orbit. In this case, the distortion is calculated using the HO density with  $b_{\rm HO}=1.621~{\rm fm^{-1}}$  and the suppression of the cross sections for the multiplets depends only very weakly on the many-particle approach and the effective YN interaction, particularly in the considered case of the shell model with the p-shell optimized interaction [3, 6] and the TD $_{\Lambda}$  approach with the Nijmengen F interacion [14].

In Figure 1 we show effects of kaon distortion in the case of  ${}^{40}_{\Lambda}{\rm K}$  calculated with two different nucleon densities. The harmonic-oscilator (HO) and Hartree-Fock (HF) forms of densities are shown in part (a) where it is apparent that the HO density, calculated with  $b_{\rm HO} =$ 1.939 fm<sup>-1</sup>, is not a realistic description, mainly in the central region of the nucleus. However, as shown in part (b) the suppression of the excitation spectrum caused by the HO and HF density does not differ too much, suggesting that the effect is given mainly by a behavior of the density in the peripheral region of the nucleus whereas its behavior inside the nucleus is irrelevant for the kaon distortion accounted for by the eikonal approximation. Note that the mean nucleus radius calculated with the HF density is 3.07 fm and that with the HO density is 2.83 fm which do not differ too much. The failure of the HO form in describing the nucleon density in the central region of the nucleus can be attributed to the simple form considered in Eq. (8) which is inadequate for the sd-shell and still heavier nuclei. A detailed study of distortion effects in electroproduction of p- and sd-shell hypernuclei was also performed in Ref. [15].

Similar effects are shown for a heavy hypernucleus  $^{208}_{\ ^{\Lambda}}\mathrm{Tl}$  in Fig. 2. Here we show distortion effects calculated with two distinct forms of HO with  $b_{\rm HO} = 3.51~{\rm fm}^{-1}$  and  $b_{\rm HO}=2.25~{\rm fm^{-1}}$ . The latter, being an extremely unrealistic description, was chosen just to demonstrate that even such very bad description of the density in the central region has only mild effects in the excitation spectrum. The mean radius calculated with these HO densities are  $\langle R \rangle = 5.22$  fm and 3.36 fm, respectively and when we compare them with the HF radius  $\langle R_{\rm HF} \rangle = 5.26$  fm we see that the former agrees well with  $\langle R_{\rm HF} \rangle$ . As this former form of the HO density is also very close to the HF density in the peripheral region, see Fig. 2(a), it is not surprising that the distortion effects are very similar to those of the HF density, see part (b). The version of HO with  $b_{\rm HO} = 2.25~{\rm fm}^{-1}$  differs quite a lot in the peripheral region and therefore the distortion effect is smaller as we see in Fig. 2(b).

We can conclude that the distortion effects amount to 40–60% for  $^{40}_{\Lambda}{\rm K}$  and 50–80% for  $^{208}_{\Lambda}{\rm Tl}$  and that they de-

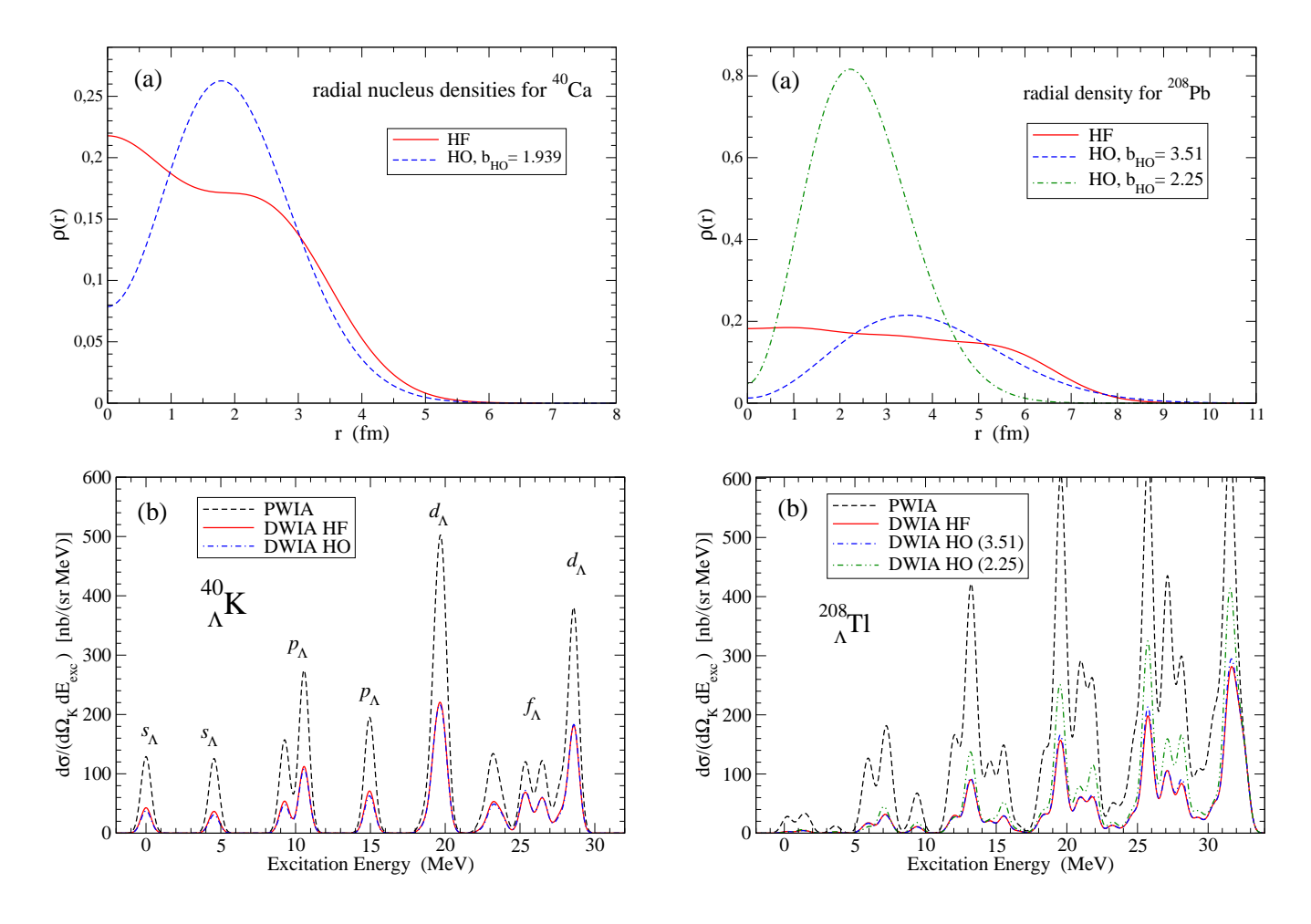


FIG. 1. Effects from kaon distortion for  $^{40}_{\Lambda}$ K. The panel (a) shows radial nucleon densities from the harmonic-oscilator parametrization (HO) with  $b_{\rm HO}=1.939~{\rm fm}^{-1}$  and the Hartree-Fock calculation (HF), both normalized to A = 40. The panel (b) compares the excitation spectra calculated in PWIA and DWIA. In the latter the kaon-nucleus optical potential is calculated using the HO and HF nucleon densities shown in (a). Calculations are performed in the Tamm-Dancoff (TD<sub> $\Lambda$ </sub>) formalism using the Nijmegen F YNG interaction with the Fermi momentum  $k_F=1.30~{\rm fm}^{-1}$  and the BS3 amplitude in the optimum on-shell approximation. The curves are plotted with FWHM = 800 keV.

pend on behavior of the nucleus density in the peripheral region rather than in the nuclear interior. Another observation is that the hypernucleus states with a more deeply bound  $\Lambda$  hyperon, e.g. in the s orbit, are more strongly affected with the kaon distortion than the states with  $\Lambda$  in higher lying orbits, e.g. d. Note also that the different strength of the kaon distortion for various states changes the shape of multiplets in the spectrum as observed in Fig. 2. In our present calculations we use the HF densities which provide a more realistic optical potential and which are obtained in the many-particle calculations being consistent with the values of OBDMEs.

FIG. 2. The same as in Fig. 1 but for  $^{208}_{\Lambda}$ Tl.

As we mentioned above, in determination of kinematics we use the hypernucleus mass shifted by excitation energy of given state:  $M_H^* = M_H^0 + E^*$  where  $M_H^0$  and  $E^*$  are the hypernucleus ground-state mass and excitation energy, respectively. Even if this mass shift is relatively very small it can change values of some particle momenta even by a few percent and therefore the elementary amplitude and the radial integrals can notably change their values. In Table I we show how a relatively tiny shift of the mass propagates into variations of the momenta, the elementary amplitude, the radial integral, and finally how it changes the cross section. The results, calculated in PWIA at photon energy  $E_{\gamma} = 1.5$  GeV, are shown for two states of  ${}^{208}_{\Lambda}{\rm Tl}$  with the same spin to see variations of the effect in dependence on  $E^*$ . Whereas changes of the momenta are proportional to the excitation energy, the radial integral reveals different effects and therefore the cross section can be less suppressed for the larger shift. The value of the radial integral is given by the overlap of the proton and  $\Lambda$  single-particle wave functions and the function proportional to the spherical Bessel function in PWIA,  $F_{LM}(\Delta B \xi) \sim j_L(\Delta B \xi)$ , see

Eq. (2). A few percent change of  $\Delta$  can vary the overlap of the functions resulting in a quite different value of  $\mathcal{R}^{LM}_{\alpha'\alpha}$ . It is also remarkable in the table that the particle momenta decrease due to the mass shift but the momentum transfer  $\Delta$  rises and that the proton momentum  $|\vec{p}_{opt}|$  significantly changes which then markedly affects the value of the elementary amplitude. The changes are also present in the transversal part  $(d\sigma_T)$  of the full cross section  $(d\sigma)$ . Note that dependence of the cross sections on the momentum transfer  $\Delta$  was also studied in the DWIA calculations of photoproduction of  $^{208}$ Tl in Ref. [11] observing noticeable effects.

	states								
	$(11.964, 8^-)$	$(18.201, 8^+)$							
$M_H^*$	0.006	0.009							
$ ec{P}_K $	-1.0	-1.6							
$\Delta$	3.0	4.6							
$ ec{p}_{opt} $	-15.7	-23.5							
$\mathrm{Re}\mathcal{F}^1_{00}$	-1.2	-4.5							
$\mathrm{Im}\mathcal{F}^1_{00}$	-31.4	-44.4							
$\mathcal{R}^{LM}_{lpha'lpha}$	$\mathcal{R}^{70}_{\alpha'\alpha}: -3.7$	$\mathcal{R}^{80}_{\alpha'\alpha}: 20.2$							
$\mathrm{d}\sigma$	-16.0	-10.6							
$d\sigma_T$	-13.2	-9.6							

TABLE I. Changes, in % with respect to the ground-state values, are due to the mass shift for two states of  $^{208}_{\Lambda} \text{Tl:}$   $(E^*[\text{MeV}],\ J_{\text{H}}^P)$ . The changes are shown for the kaon momentum  $|\vec{P}_K|$ , momentum transfer  $\Delta=|\vec{\Delta}|$ , proton optimum momentum  $|\vec{p}_{opt}|$ , the spin-flip elementary amplitude with zero projections and the relevant radial integrals for dominant transitions  $0h_{11/2} \to 0d_{5/2}$  and  $0h_{11/2} \to 0f_{5/2}$ . The full (d $\sigma$ ) and transversal (d $\sigma_T$ ) cross sections [13] decrease by 10–16%.

Despite the fact that the cross sections for various states can change in different way, as one can see in Table I, the overall effect in the excitation spectrum is monotonously rising with the excitation energy as shown in Fig. 3. Therefore, both the  $d_{\Lambda}$  and  $f_{\Lambda}$  peaks change similarly by about 16% even if the cross section for the state (18.201, 8<sup>+</sup>) changes only by 10.6%. This is because of dominance of the first state (11.964, 8<sup>-</sup>) in the  $d_{\Lambda}$  peak whereas the  $f_{\Lambda}$  peak is dominated by the (18.316. 9<sup>+</sup>) state with the cross section changed by 16.3%.

We can conclude that the effects from the hypernucleus-mass shift are quite important correction to the cross section of high-lying hypernucleus states. In the considered kinematical region the mass shift suppresses the cross sections.

### A. On-shell approximation

In previous calculations we used the optimum on-shell approximation [13] with the optimum proton momentum calculated from the two-body energy conservation in the

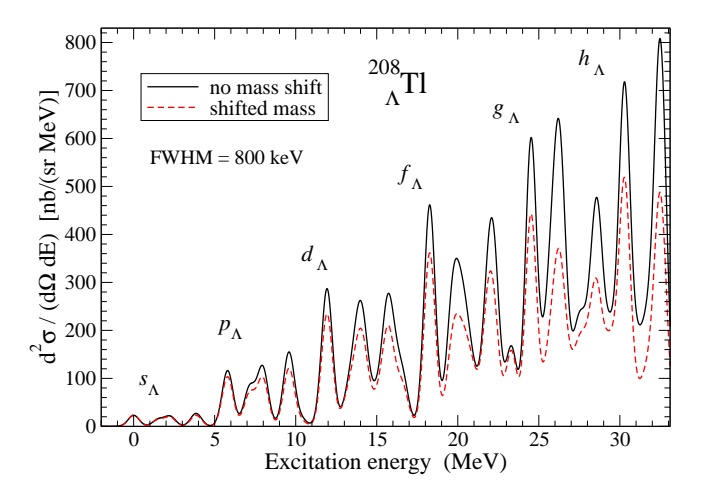


FIG. 3. The excitation spectra of  $^{208}_{~\Lambda} \rm Tl$  calculated in PWIA without and with the shift of hypernucleus mass due to the excitation energy. The calculations are for  $E_{\gamma}=1.5~\rm GeV$  and  $\theta_{K\gamma}=8^{\circ}$  with the BS3 elementary amplitude in the optimum on-shell approximation.

laboratory frame (the nucleus is in rest)

$$E_{\gamma} + \sqrt{m_p^2 + (\vec{p}_{opt})^2} = \sqrt{m_{\Lambda}^2 + |\vec{\mathsf{P}}_{\mathsf{K}}|_{mb}^2} + \sqrt{m_{\Lambda}^2 + (\vec{\Delta} - \vec{p}_{opt})^2}, \quad (9)$$

where  $m_p$  and  $m_\Lambda$  are the proton and  $\Lambda$  masses, respectively,  $E_\gamma$  is the photon energy, and  $|\vec{P}_K|_{mb}$  is magnitude of the kaon lab momentum computed from the manybody energy conservation. This equation assures that the elementary amplitude is on shell but we have to chose a value of the angle  $\theta_{\Delta p}$  between the proton momentum and the momentum transfer. Kinematics in the coplanar case  $(\Phi_K = \Phi_p)$  is depicted in Fig. 4. In previous calculations [13, 14], we had chosen  $\theta_{\Delta p} = 180^\circ$  as then both proton and  $\Lambda$  momentum received the minimum value at given kinematics.

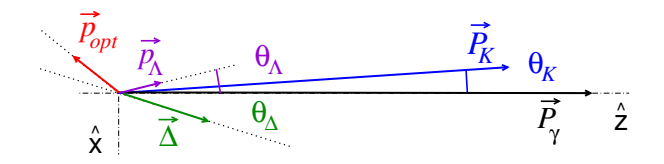


FIG. 4. Kinematics of the elementary process in the coplanar case with the axis  $\hat{y}$  oriented rearwards the page. The angle  $\theta_{\Delta p}$  between the proton optimum momentum  $\vec{p}_{opt}$  and the momentum transfer  $\vec{\Delta} = \vec{P}_{\gamma} - \vec{P}_{\rm K}$  has a general value.

In the present calculations we elaborate this approach assuming that the magnitude of  $\vec{p}_{opt}$  equals the mean momentum of the proton in the single-particle state of

the dominant transition. This mean value,  $p_{mean} =$  $\sqrt{2\mu \langle T_{kin} \rangle}$  with the reduced mass  $\mu$ , is calculated for each hypernucleus state from the proton single-particle wave function that corresponds to the dominant value of OBDME. The mean value of the kinetic-energy operator  $\langle T_{kin} \rangle$  is evaluated directly from its definition differentiating numerically the radial wave functions. Having fixed the magnitude of the proton momentum in Eq. (9),  $|\vec{p}_{opt}| = p_{mean}$ , we can calculate the angle  $\theta_{\Delta p}$  and if it acquires a physical value, particularly  $\cos \theta_{\Delta p} \geq -1.0$ , we can use this value of the proton momentum in the calculations. In the case the angle is nonphysical,  $\cos \theta_{\Delta p}$ -1.0, we can calculate  $|\vec{p}_{opt}|$  with  $\cos \theta_{\Delta p} = -1.0$  as before, which is the minimal value at given kinematics, and because in this case  $p_{mean}$  is still smaller this value of  $|\vec{p}_{opt}|$  is a good substitution for  $p_{mean}$ .

Since many hypernucleus states, especially the low lying states, have nonphysical values of  $\theta_{\Delta p}$  and the values of  $p_{mean}$  are in general close to  $|\vec{p}_{opt}|$  with  $\cos \theta_{\Delta p} = -1.0$  the new and old variants of the optimum on-shell approximation do not differ too much.

To summarize the variants of the optimum on-shell ap-

proximation:

- a) previous version: the angle is chosen as  $\theta_{\Delta p} = 180^{\circ}$  and the magnitude of  $\vec{p}_{opt}$  calculated;
- b) elaborated version: the magnitude is specified as  $|\vec{p}_{opt}| = p_{mean}$  and the angle  $\theta_{\Delta p}$  calculated. If the angle is physical we use this otherwise we use the variant a). In the following we are going to use the variant b) and denote it as "on-shell approximation".

#### B. Fermi motion effects

Dependence of the cross sections on various values of the proton effective momentum was shown and discussed for the p-shell hypernuclei in Ref. [13]. In Figures 5 and 6 we show these Fermi motion effects for several states  $(E^*[\text{MeV}], J_{\text{H}}^P)$  of the heavy hypernucleus  $^{208}_{\Lambda}\text{Tl}$  in dependence on the kaon angle with respect to the electron beam  $\theta_{\text{Ke}}$  and on the photon laboratory energy  $E_{\gamma}$ , respectively.

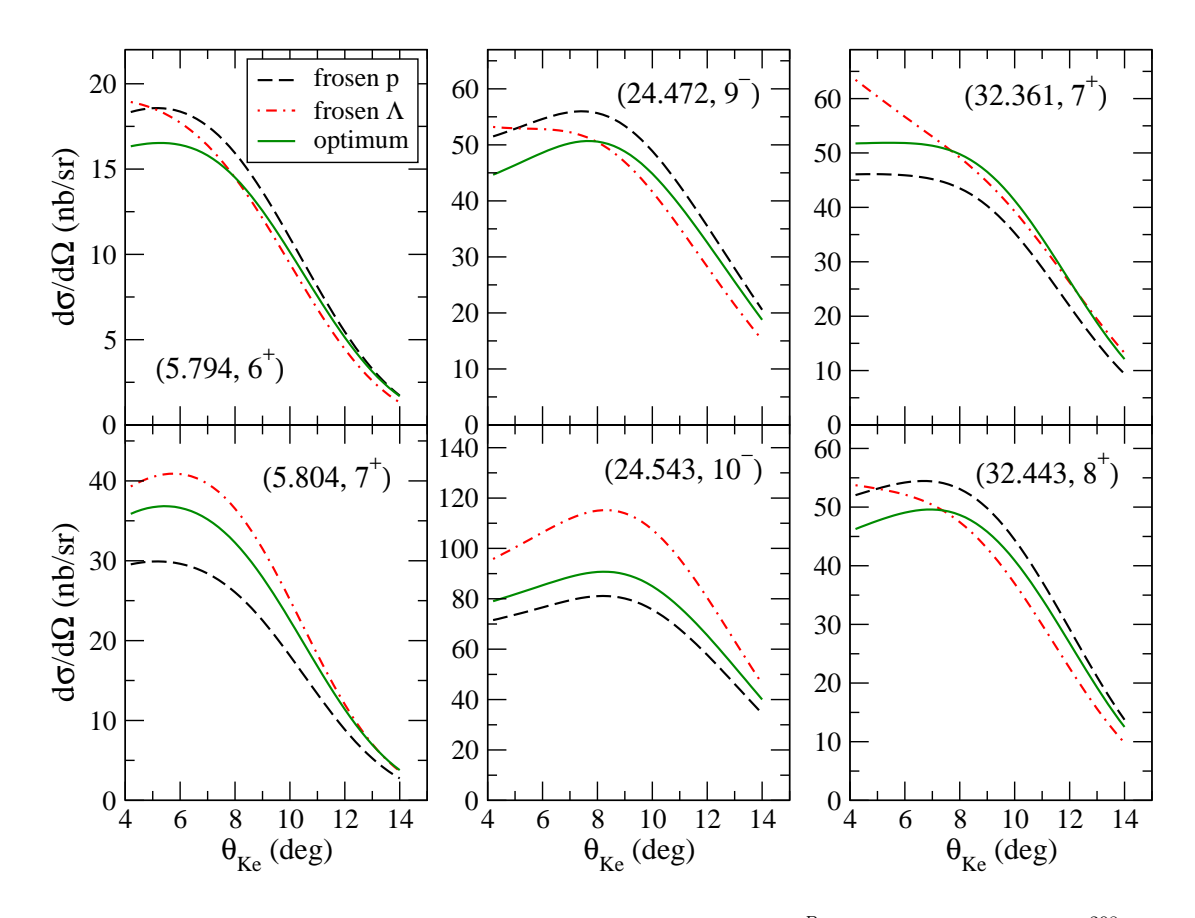


FIG. 5. Angular dependence of the cross sections for selected states ( $E^*[\text{MeV}]$ ,  $J_{\text{H}}^P$ ) in electroproduction of  $^{208}_{\Lambda}\text{Tl}$ . The results are shown for various values of the effective proton momentum,  $\vec{p}_{eff} = 0$  (frosen p),  $\vec{p}_{eff} = -\vec{\Delta}$  (frosen  $\Lambda$ ), and  $\vec{p}_{eff} = \vec{p}_{opt}$  (optimum). The calculations were performed with the elementary amplitude BS3 [28] at  $E_{\gamma} = 1.5$  GeV.

The biggest differences of the cross sections, mostly observed between the boundary cases of "frosen" proton and  $\Lambda$ , are at small kaon angles amounting about 20–30%. The energy dependence of the effects reveals a resonant-like structure in some cases and more pronounced effects are observed for energies below 2 GeV. Similarly as in the case of lighter hypernuclei one can see that the nature of the effects is very similar for the states  $6^+$ ,  $9^-$ , and  $8^+$  and for  $7^+$ ,  $10^-$ , and  $7^+$ , particularly the sequence of the curves is almost identical. The similarity of the effects inside these two groups of states is given by the selection rule discussed in Ref. [13]. This rule says that contributions from the longitudinal mode of the virtual photon ( $\lambda = 0$ ) are important only for the states with specific spin and parity. Let us show this in the example: both states  $(5.794, 6^+)$  and  $(5.804, 7^+)$  are dominated by the proton  $\rightarrow \Lambda$  transition  $0h \rightarrow 0p$  which means that L=6 in Eq. (1). As the leading contribution to the reduced amplitude with  $\lambda=0$  comes from the spin-flip elementary amplitude with S=1 and  $\eta=0$  and the biggest value of the radial integral is for M=0 the corresponding Clebsch-Gordan coefficients in Eq. (1) are  $\mathsf{C}_{6010}^{60}=0$  and  $\mathsf{C}_{6010}^{70}=\sqrt{7/13}$ . The longitudinal contributions in the case of  $7^+$  then make the frosen- $\Lambda$  cross section mostly larger than that for the case with the stationary proton contrary to the case of the state  $6^+$ . This longitudinal contribution also makes the pronounced resonant structures in the energy dependent cross sections in Fig. 6. These observations demonstrate importance of the contributions from the longitudinal and transverse-longitudinal interference terms in the electroproduction cross section [13].

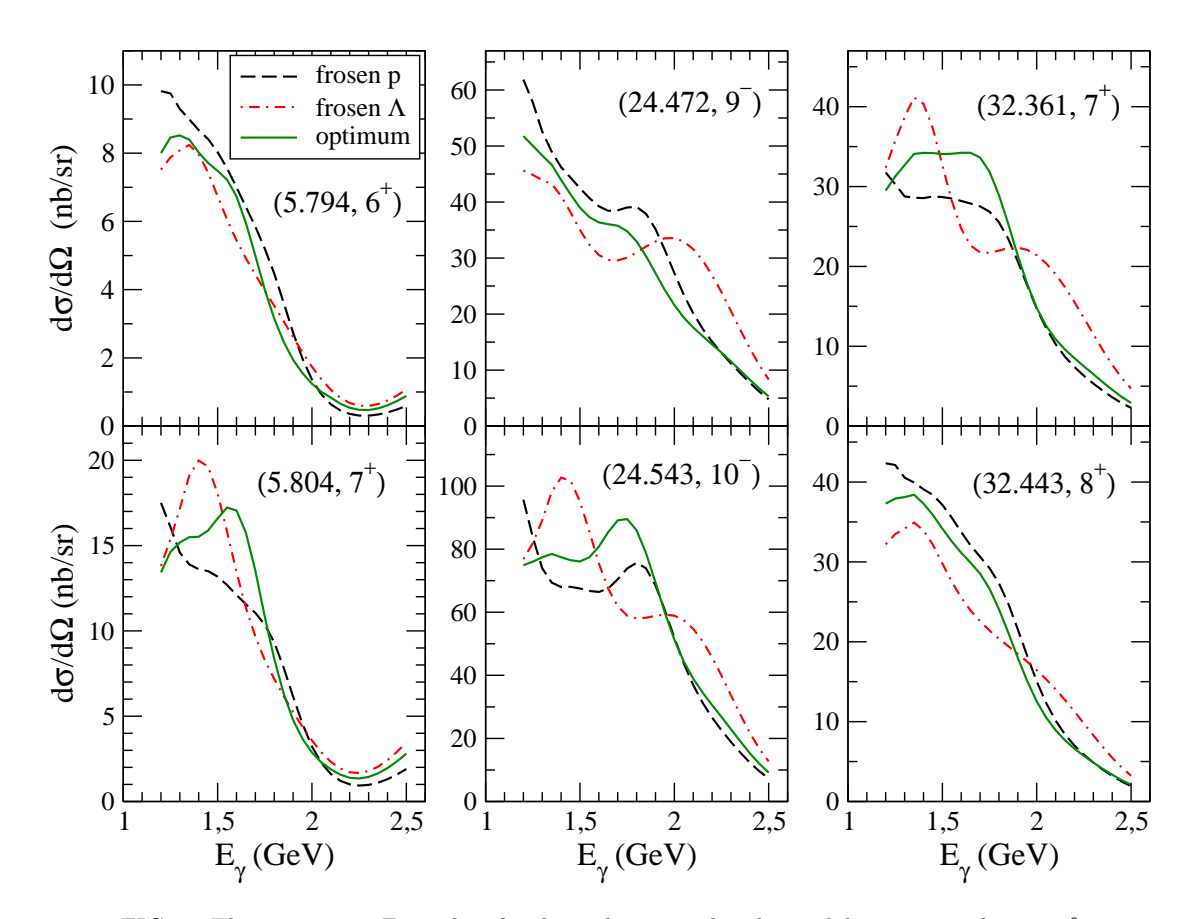


FIG. 6. The same as in Fig. 5 but for dependence on the photon lab energy at  $\theta_{\rm Ke} = 11^{\circ}$ .

The results with the optimum momentum mostly lie within the limit cases with the frosen proton and  $\Lambda$  which is given by values of the proton and  $\Lambda$  momenta. For example, at  $E_{\gamma}=1.5$  GeV and  $\theta_{Ke}=11^{\circ}$  the pro-

ton and  $\Lambda$  momenta for the state (5.804,  $7^+$ ) are 0 and 392 MeV/c for the frosen proton, 292 and 0 MeV/c for the frosen  $\Lambda$ , and 207 and 162 MeV/c for the optimum proton momentum case, respectively. Note that the re-

sults in Figs. 5 and 6 are calculated with the elementary amplitude BS3 [28] which has a more abundant energy structure than the Saclay-Lyon amplitude as discussed in Ref. [13].

# IV. DISCUSSION OF EXCITATION SPECTRA FOR MEDIUM- AND HEAVY-MASS HYPERNUCLEI

### A. ${}^{40}_{\Lambda}$ K and ${}^{48}_{\Lambda}$ K

The excitation spectra in electroproduction of  ${}^{40}_{\Lambda}{\rm K}$  and  ${}^{48}_{\Lambda}{\rm K}$  were already discussed in Ref. [14]. It was shown how much the spectra depend on the Fermi momentum  $k_F$ , used to parametrize the YNG Nijmegen F interaction, and on the elementary amplitudes SLA and BS3. We have also compared the results obtained in two various approaches, namely in TD<sub>\Lambda</sub> and the Equation of Motion Phonon Method (EMPM<sub>\Lambda</sub>). These results were obtained using the chiral NNLO<sub>sat</sub> NN+NNN potential [29] and the kaon distortion was computed with the HO nucleus density and  $b_{\rm HO}=1.939~{\rm fm}^{-1}$  [14].

In the present paper we show results calculated in the  $TD_{\Lambda}$  approach using the D16+DDT interaction with  $C_{\rho} = 2000 \text{ MeV} \cdot \text{fm}^6 \text{ in eq. (4)}$  and the kaon distortion is included using the optical potential constructed with the HF densities of the target nuclei obtained in the HF approach. The upgraded results calculated with the BS3 amplitude in the on-shell approximation and with two YNG interactions, Jülich A (JA) and Nijmegen F (NF), are compared with the previous calculations in Figs. 7 and 8. Note that the old results were calculated with  $k_F=1.25~{\rm fm^{-1}}$  and the new ones with 1.30 and 1.34 fm<sup>-1</sup> for  $^{40}_{~\Lambda}{\rm K}$  and  $^{48}_{~\Lambda}{\rm K}$ , respectively. Differences in the NN interaction, the value of  $k_F$  and using the JA YNG interaction make changes in the excitation spectra where the production strength is re-distributed into diverse structures. However, the magnitudes of the peaks, which are sensitive especially to the elementary amplitude and kinematics, mostly do not differ too much for various interactions. The results presented in Figs. 7 and 8 demonstrate a variety of predictions for the experiment E12-15-008 in preparation at Jefferson Lab.

# $\mathbf{B}$ . ${}^{52}_{\Lambda}\mathbf{V}$

We also provide predictions of the excitation spectrum in the reaction  $^{52}{\rm Cr}(e,e'K^+)^{52}_{\Lambda}{\rm V}$  and compare them with the older calculation in Ref. [10]. This older result presented in Ref. [10], Fig. 7, is for photoproduction in kinematics  $E_{\gamma}=1.3$  GeV and  $\theta_{K\gamma}=3^{\circ}$  and with the SLA amplitude in the frosen-proton approximation. The spectrum clearly shows separated multiplets with the  $\Lambda$  hyperon in the s,~p,~d, and f orbit. The major peaks are based on the conversion of protons in the  $0f_{7/2}$  orbit into the  $\Lambda$  bound in the given  $l_{\Lambda}$  orbit. Note that the dom-

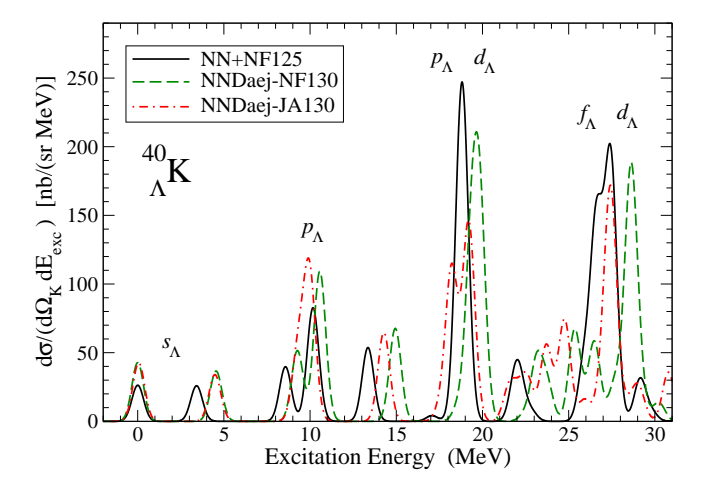


FIG. 7. The previous result for  $^{40}\Lambda{\rm K}$  with the BS3 amplitude in the optimum on-shell approximation [14] (NN+NF125) is compared with the upgraded calculations using the D16+DDT interaction and the NF (NNDaej-NF130) and JA (NNDaej-JA130) YNG interactions, both with  $k_F=1.30$  fm<sup>-1</sup>. The kaon distortion is included using the HF density of  $^{40}{\rm Ca}$ . The curves are plotted with FWHM = 800 keV.

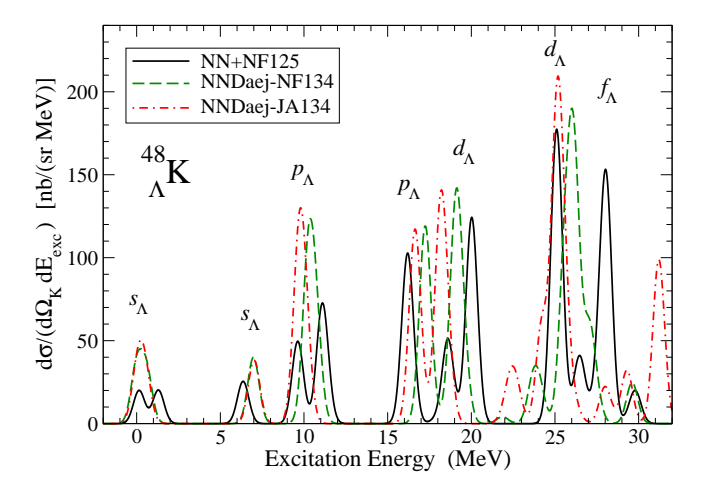


FIG. 8. The same as in Fig. 7 but for  ${}^{48}_{\Lambda}{\rm K}$  and  $k_F=1.34$  fm<sup>-1</sup>.

inant unnatural-parity peaks  $(4^-, 5^+, 6^-, 7^+)$  are with  $J_{max} = L_{max} + 1$ . The other well separated and important peaks are based on the proton hole  $d_{3/2}^{-1}$  [10].

The results presented here are for electroproduction in kinematics  $E_i = 1.6$  GeV,  $E_f = 0.3$  GeV,  $\theta_e = 4.5^{\circ}$ ,  $\theta_{Ke} = 4.04^{\circ}$ , and  $\Phi = 180^{\circ}$  giving photoproduction kinematics  $E_{\gamma} = 1.3$  GeV,  $Q^2 = 0.003$  (GeV/c)<sup>2</sup>,  $\varepsilon = 0.362$ ,  $\theta_{\gamma e} = 1.04^{\circ}$ , and  $\theta_{K\gamma} = 3.0^{\circ}$ , quite close to that in Ref. [10]. The kaon distortion is included using the HF density for <sup>52</sup>Cr and the OBDMEs are determined within the HF+TD<sub> $\Delta$ </sub> approach using the NN interaction

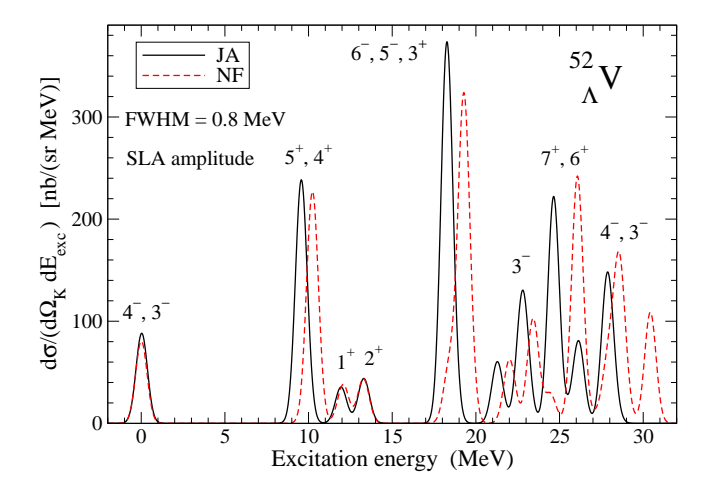


FIG. 9. Excitation spectra for electroproduction of  $^{52}_{\Lambda}\text{V}$  calculated in the TD<sub>\Lambda</sub> approach with the Jülich A (JA) and Nijmegen F (NF) YNG interactions and with the elementary amplitude SLA in the frosen-proton approximation.

D16+DDT with  $C_{\rho} = 2000 \text{ MeV} \cdot \text{fm}^6$  in eq.(4) and JA and NF YNG interactions with  $k_F = 1.34 \text{ fm}^{-1}$ .

In Figure 9 we show results calculated with the SLA amplitude in the frosen-proton approximation  $(p_{eff} = 0)$ and the JA and NF YNG interactions, which can be compared with the results in Fig. 7 of Ref. [10]. One can observe that the main three peaks in the JA result are of similar magnitude and position as in Ref. [10]. In the new calculations, these main peaks are especially formed by the following states  $(E^*[\text{MeV}], J_H^P)$  dominantly populated by the single-particle transitions  $nl_j \to n'l'_{j'}$ : (0.0 MeV, 4<sup>-</sup>) with  $0f_{7/2} \rightarrow 0s_{1/2}$  and (0.078 MeV, 3<sup>-</sup>) with  $0f_{7/2} \rightarrow 0s_{1/2}$  for the ground-state doublet; (9.497 MeV,  $5^+$ ) with  $0f_{7/2} \rightarrow 0p_{3/2}$  and (9.633 MeV,  $4^+$ ) with  $0f_{7/2} \rightarrow 0p_{3/2}$  and  $0p_{1/2}$  for the second main peak;  $(18.181 \text{ MeV}, 6^-) \text{ with } 0f_{7/2} \rightarrow 0d_{5/2} \text{ and } (18.313 \text{ MeV},$ 5<sup>-</sup>) with  $0f_{7/2} \rightarrow 0d_{3/2}$  and  $0d_{5/2}$  for the third peak; and (24.619 MeV, 7<sup>+</sup>) with  $0f_{7/2} \rightarrow 0f_{7/2}$  and (24.687 MeV,  $6^+$ ) with  $0f_{7/2} \rightarrow 0f_{7/2}$  and  $0f_{5/2}$  for the fourth main peak. Exceptions are the states:  $(11.942 \text{ MeV}, 1^+)$ with dominant transition  $1s_{1/2} \rightarrow 0s_{1/2}$ , (13.327 MeV,  $2^{+}$ ) with  $0d_{3/2} \rightarrow 0s_{1/2}$ , (27.814 MeV,  $4^{-}$ ) with  $0d_{5/2} \rightarrow$  $0p_{3/2}$ , and (20.008 MeV, 3<sup>-</sup>) with  $0d_{5/2} \to 0p_{3/2}$  and  $0p_{1/2}$ . Moreover the part of the spectrum with  $\Lambda$  in f orbit reveals quite different distribution of the production strength than in Fig. 7 of Ref. [10]. Also the strength in between the main peaks, based on the proton hole in  $d_{3/2}^{-1}$ , is missing in our result based on the TD<sub> $\Lambda$ </sub> approach. Possible explanation is that we would need to use an approach beyond  $TD_{\Lambda}$ , which includes coupling to the nuclear core excitation, in order to obtain this strength. An example of such approach is  $EMPM_{\Lambda}$ , see Ref. [14] for more detailed discussion.

In Figure 10 we compare the results calculated with the

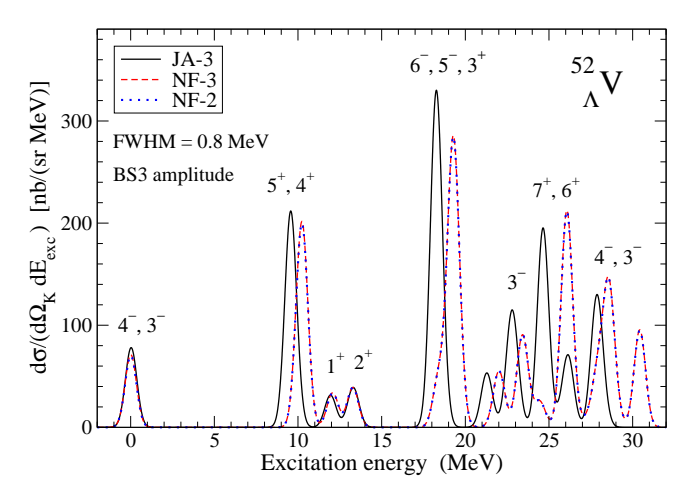


FIG. 10. The same as in Fig. 9 but with the BS3 amplitude in the on-shell approximation (JA-3 and NF-3). The result NF-3 is compared with previous "optimum on-shell approximation" (NF-2).

BS3 amplitude in the on-shell approximation for the JA and NF YNG interactions. The only difference of shapes of spectra in Figs. 9 and 10 for a given YNG interaction is in magnitudes of the peaks which depend on the elementary amplitude and kinematics (on-shell or frosen-proton approximation). Note that in the frosen-proton approximation the proton and  $\Lambda$  momenta are 0 and 362 MeV/c whereas in the on-shell approximation they are 181 and 105 MeV/c (for the ground state), respectively. This difference might seem small but it does play a role as shown in Figs. 5 and 6 and in Ref. [13]. In case of NF we also compare the new on-shell result (NF-3) with the previous optimum on-shell approximation (NF-2) used before in Refs. [13] and [14]. As we have already mentioned the difference between these spectra is almost negligible. This is because although the magnitudes of the cross sections for separate hypernucleus states differ by about 1% the sign of the differences for various states in a multiplet is scattered on both sides (positive/negative) and therefore the overall shape of the peaks composed from several states remains almost unchanged. The small difference of the cross sections can be attributed to a small difference between the proton momentum  $p_{opt}$  with  $\cos \theta_{\Delta p} = -1$ and  $p_{mean}$  for the proton single-particle wave function of the dominant transition, see Subsect. 3.1.

The results in Fig. 10 demonstrate a measure of sensitivity of the spectra to using different forms of the effective YNG interactions in the DWIA calculations which is comparable to the width of the peaks (FWHM = 800 keV). We therefore presume that analysis of a good quality experimental spectrum obtained in the reaction  $^{52}{\rm Cr}(e,e'K^+)^{52}_{\Lambda}{\rm V}$  could help in a more precise determination of the spin-dependent part of the YNG interaction.

In this subsection we discuss results for the reaction  $^{208}{\rm Pb}(e,e'K^+)^{208}{\rm Tl}$  where both  $^{208}{\rm Pb}$  and  $^{208}{\rm Tl}$  are very heavy systems with 126 neutrons which act as spectators in the impulse approximation still affecting kinematics of the reaction. The mass of the ground state of  $^{208}{\rm Pb}$  is taken to be  $M_{Pb}^N=193.68769~{\rm GeV}$  and that of  $^{208}{\rm Tl}$  is estimated to be  $M_{Tl}^H=M_{Pb}^N-m_p+m_\Lambda+\varepsilon_p-\varepsilon_\Lambda\doteq 193.8482~{\rm GeV}$  considering that the difference of the binding energies is  $m_\Lambda-m_p+\varepsilon_p-\varepsilon_\Lambda\approx 160.5~{\rm MeV}.$  Determining precise values of the masses is quite important, remind the discussion of sensitivity of the cross sections to the hypernucleus mass in Sect. 3.

The cross sections of  $^{208}\Lambda Tl$  are calculated in the HF+TD $_{\Lambda}$  approach using the NN interaction D16+DDT with  $C_{\rho}=4000$  MeV·fm<sup>6</sup> and various YNG interactions and elementary amplitudes. The aim is to show a variety of predictions for the planned experiment E12-20-013 at JLab [8]. The results are for the new kinematics in Hall C [30],  $E_i=2.24$  GeV,  $E_f=0.74$  GeV,  $\theta_e=8^{\circ}$ ,  $\theta_{Ke}=11^{\circ}$ , and  $\Phi_K=180^{\circ}$ , which gives  $E_{\gamma}=1.5$  GeV,  $|\vec{p}_{\gamma}|=1.511$  GeV/c,  $Q^2=0.0323$  (GeV/c)<sup>2</sup>,  $\theta_{\gamma e}=3.9^{\circ}$ ,  $\varepsilon=0.591$ ,  $\Gamma=0.0140$  sr<sup>-1</sup>GeV<sup>-1</sup>,  $\theta_{K\gamma}=7.1^{\circ}$ , and in the case of the ground state:  $|\vec{P}_K|_{mb}=1.245$  GeV/c,  $|\vec{\Delta}|=315$  MeV/c,  $\theta_{\Delta\gamma}=29.2^{\circ}$ ,  $|\vec{p}_{opt}|=205$  MeV/c, and  $|\vec{p}_{\Lambda}|=110$  MeV/c. The kinematics is in the laboratory frame.

The ground state of the target nucleus <sup>208</sup>Pb is  $J_A^{P_A} =$ 0<sup>+</sup> and its wave function is represented by the HF Slater determinant. We assume that  $^{208}_{\Lambda}$ Tl can be understood as  $\Lambda$  bound in the core nucleus  $^{207}$ Tl which is a spectator in the impulse approximation. Therefore, it is important to describe well also the core nucleus in our approach. Within the HF method, energy spectrum of <sup>207</sup>Tl can be estimated from the proton single-particle energies  $\varepsilon_p$ . If we set the last occupied proton level (i.e.  $0h_{11/2}$ ) to 0.0 MeV we can take the relative energies of the following occupied levels  $(2s_{1/2},\ 1d_{3/2},\ 1d_{5/2},\ 0g_{7/2})$  with respect to  $0h_{11/2}$  as an estimate of the low-lying energy spectrum of  $\frac{11}{2}$ ,  $\frac{1}{2}$ ,  $\frac{1}{2}$ ,  $\frac{3}{2}$ ,  $\frac{5}{2}$ ,  $\frac{7}{2}$  states in  $^{207}$ Tl. Such spectrum of the core nucleus obtained within our HF calculation is shown in the left column in Fig. 11 and denoted as "original" because it was obtained with the original form of the NN interaction. This original spectrum is compared with the phenomenological one in the right column which was obtained from experiments [31–33]. Note that the fifth single-particle state  $\frac{7}{2}^+$  was observed in the  $^{208}{\rm Pb}(\gamma,p)$  and  $^{208}{\rm Pb}(e,e'p)$  reactions [32, 33] and was also considered in the calculations by Motoba and Millener [8]. However, this state was not seen in the collision of two <sup>208</sup>Pb nuclei [31]. Instead the state  $\frac{17}{2}$  at 3.813 MeV was observed.

The comparison demonstrates that the empirical spectrum is quite significantly squeezed down with respect to the theoretical (original) result and the ground-state in the theoretical spectrum  $\frac{11}{2}^-$  lies above the state  $\frac{3}{2}^+$ 

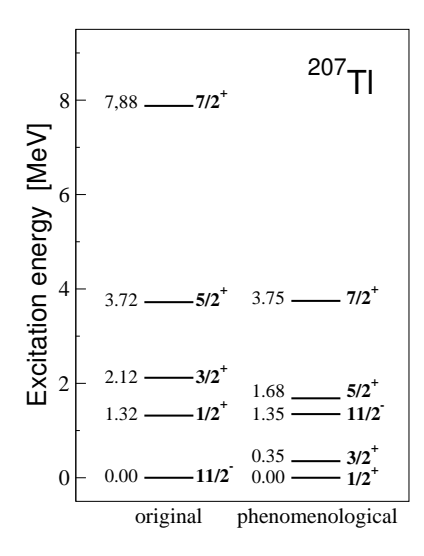


FIG. 11. The spectrum of the core nucleus  $^{207}{\rm Tl}$  calculated in the HF method using the D16+DDT NN interaction with  $C_{\rho}=4000~{\rm MeV\cdot fm^6}$  and denoted as "original" in the left column is compared with phenomenological values obtained in experiments [31–33] (the right column). The energies are in MeV.

in the phenomenological spectrum. The phenomenological spectrum reflects that, in fact, the effective NN interaction should be modified. In this study, we mimic such effect by changing the proton  $2s_{1/2}$ ,  $1d_{3/2}$ ,  $1d_{5/2}$ ,  $0g_{7/2}$  single-particle energies  $\varepsilon_p$  in order to reproduce the phenomenological  $\frac{1}{2}^+$ ,  $\frac{3}{2}^+$ ,  $\frac{11}{2}^-$ ,  $\frac{5}{2}^+$ , and  $\frac{7}{2}^+$  energies of  $^{207}$ Tl. These values of  $\varepsilon_p$  enter the TD<sub> $\Lambda$ </sub> calculation (see Eq. (11) in [14]) and, therefore, modify OBDME.

The excitation spectra in electroproduction of  $^{208}_{\Lambda}$ Tl calculated with the original and phenomenological spectrum of <sup>207</sup>Tl are shown in Fig. 12. Both results were obtained using the BS3 amplitude in the on-shell approximation and the Nijmegen F YNG interaction with  $k_{\rm F} = 1.34 \; {\rm fm^{-1}}$ . The results are for kinematics of the experiment E12-20-013 in Hall C. One can see that changing the spectrum of <sup>207</sup>Tl results in a systematical shift of positions of the main peaks to larger energies. In general, the shape of the new excitation spectrum has changed with the phenomenological single-particle energies suggesting that ordering of some hypernucleus states has changed as well as the production cross sections. Note that assuming the phenomenological spectrum of <sup>207</sup>Tl means a modification of the cross sections via the values of OBDME.

A strength of the  $\operatorname{proton}(\alpha) \to \Lambda(\alpha')$  transition is given by the reduced matrix element of the one-body transition operator (OBDME)  $(\Phi_{\mathsf{H}}|| \left[b_{\alpha'}^+ \otimes a_{\alpha}\right]^J || \Phi_{\mathsf{A}})$  and the radial integral  $\mathcal{R}^{LM}_{\alpha'\alpha}$  where the sum in Eq. (1) runs over a model space given by  $\alpha \equiv (n \, l \, j)_{\mathsf{p}}$  and  $\alpha' \equiv (n' l' j')_{\Lambda}$ . In case of heavy hypernuclei the model space is big and its dimension is restricted by a considered accu-

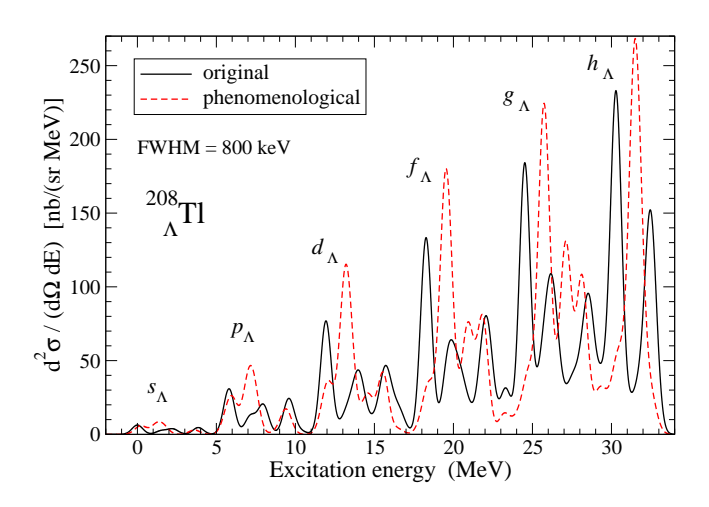


FIG. 12. The excitation spectrum in  $^{208}{\rm Pb}(e,e'K^+)^{208}_{~\Lambda}{\rm Tl}$  obtained consistently with the original and phenomenological spectrum of  $^{207}{\rm Tl}$  shown in Fig. 11.

racy. We compared the results for  $^{208}\Lambda$ Tl calculated only with the transitions satisfying  $|OBDME| \leq 0.001$  and  $|OBDME| \leq 0.0001$  and have found a tiny differences. Therefore we use the former restriction in our calculations. Moreover, in the sum typically one up to five transitions dominate and therefore one can say that the given

hypernucleus state is populated by a particular transition  $\alpha \to \alpha'$  with J, L, and S. Note that the following triangle conditions must be fulfilled for the quantum numbers:  $\Delta(l',l,L), \, \Delta(J_{\mathsf{H}},J_{\mathsf{A}},J), \, \Delta(j',j,J),$  and  $\Delta(J,L,S)$  with  $J_{\mathsf{A}}=0$  and S=0,1 for the transitions without and with spin flip, respectively. Moreover, the orbital momenta must respect the parity of the final state, i.e.  $P_{\mathsf{H}} \cdot P_{\mathsf{A}} = (-1)^L$  and l+l'+L must be an even number. The right single-particle quantum numbers to couple to the core nucleus must also satisfy  $\Delta(J_{\mathsf{c}},J_{\mathsf{H}},j'), \, \Delta(J_{\mathsf{c}},J_{\mathsf{A}},j), \, P_{\mathsf{c}} \cdot P_{\mathsf{A}} = (-1)^l,$  and  $P_{\mathsf{c}} \cdot P_{\mathsf{H}} = (-1)^{l'}.$ 

The dominant transitions for selected hypernucleus states with the corresponding quantum numbers are shown in Tables II and III. We also show the cross sections and the states in the "original" and "phenomenological" spectrum of the core  $^{207}\mathrm{Tl}$  which can be used to build up the ground state of  $^{208}\mathrm{Pb}$  and the states of  $^{208}\mathrm{Tl}$ . In Table II we compare the first and second doublet based on the ground and first excited states of the core nucleus. In the case of the original spectrum the first hypernucleus doublet is based on the ground state  $\frac{11}{2}^-$  of  $^{207}\mathrm{Tl}$  and the second doublet on the excited state  $\frac{11}{2}^+$  at 1.317 MeV. This excitation energy then gives the splitting about 1.52 MeV of the doublets. Analogous situation is in the case of the phenomenological spectrum with the states  $\frac{1}{2}^+$  and  $\frac{3}{2}^+$  split only by 0.351 MeV giving the moderate doublet splitting  $\approx 0.28$  MeV.

original spectrum of <sup>207</sup> Tl										
core	proton	hyperi	nucleus	cross sections						
$E_{\sf c}  J_{\sf c}^{P_{\sf c}}$	$n \ l \ j$	n' $l'$ $j'$	$E_{H}$	$J_{H}^{P_{H}}$	J L	S	$[\mathrm{nb/sr}]$			
$0.000 \frac{11}{2}^{-}$	$0\ 5\ \frac{11}{2}$	$0 \ 0 \ \frac{1}{2}$	0.000	$6^-$	6 5	1	3.66			
$0.000 \frac{11}{2}^-$	$0\ 5\ \frac{11}{2}$	$0 \ 0 \ \frac{1}{2}$	0.003	$5^{-}$	5 5	0,1	1.74			
$1.317 \frac{1}{2}^+$	$2 \ 0 \ \frac{1}{2}$	$0 \ 0 \ \frac{1}{2}$	1.485	$0_{+}$	0 0	0	0.03			
$1.317 \frac{1}{2}^+$	$2\ 0\ \frac{1}{2}$	$0 \ 0 \ \frac{1}{2}$	1.519	$1^+$	1 0	1	2.04			

phenomenological spectrum of <sup>207</sup> Tl										
CO	re	pro	on	Λ		hyperi	nucleus	3		cross sections
						$E_{H}$				$[\mathrm{nb/sr}]$
0.000	$\frac{1}{2}^{+}$	2 0	$\frac{1}{2}$	0 0	$\frac{1}{2}$	0.000	$0_{+}$	0 0	0	0.03
0.000	$\frac{1}{2}^{+}$	2 0	$\frac{1}{2}$	0 0	$\frac{1}{2}$	0.034	$1^+$	1 0	1	2.07
0.351	$\frac{3}{2}^{+}$	1 2	$\frac{3}{2}$	0 0	$\frac{1}{2}$	0.313	$2^+$	2 2	0,1	2.08
0.351	$\frac{3}{2}$ +	1 2	$\frac{3}{2}$	0 0	$\frac{1}{2}$	0.319	$1^+$	1 2	1	1.16

TABLE II. Doublets of hypernuclear states are shown with the quantum numbers of dominant transitions  $p \to \Lambda$ , the cross sections, and the corresponding states of the core nucleus. The cases with the "original" and "phenomenological" spectrum of the core <sup>207</sup>Tl are compared.

larger cross section in accord with the rule that the state with the maximum spin in the multiplet is populated most strongly. Another well known fact is that at small kaon angles, considered in electroproduction of hypernuclei, the elementary production is dominated by its spin-flip (S=1) part. Therefore, the hypernucleus states with mere S=0 are only weakly populated whereas those with S=1 have significant cross sections. This dominance of the spin-flip amplitude is clearly seen in the second and first doublet of the upper and lower part of the table, respectively. This dominance also makes the difference of the ground-state cross sections for the original and phenomenological spectrum where the former is dominantly populated by the core-nucleus state  $\frac{11}{2}$  allowing S=1 but the latter is given by the state  $\frac{11}{2}$  requiring S=0.

In Table III we show the multiplets with  $\Lambda$  in the p

and d orbits, see also Fig. 12. It is apparent again that the maximum spin states  $7^+$  and  $8^-$  dominate the  $p_{\Lambda}$ and  $d_{\Lambda}$  multiplets, respectively, in both computational approaches. All transitions shown in Table III are based on the proton hole in the  $0h_{11/2}$  orbit which corresponds to the ground state of the core nucleus in the approach with the original spectrum but to the excited state at 1.348 MeV in the phenomenological spectrum. The difference 1.348 MeV then makes the shift of the main  $p_{\Lambda}$ and  $d_{\Lambda}$  peaks observed in Fig. 12. Remind that due to the selection rule the longitudinal parts of the cross section obtain significant contributions from the spin-flip amplitude (S = 1) only for the states  $7^+$ ,  $8^-$ , and  $6^$ whereas the other states  $6^+$ ,  $7^-$ , and  $5^-$  receive their leading contributions only from the non spin-flip part of the elementary amplitude which is weaker in the studied kinematical region. This is also one of the reasons why the cross sections for the states 7<sup>+</sup> and 8<sup>-</sup> are so big.

original spectrum of <sup>207</sup> Tl									
	proton							cross sections	
$E_{c}  J_{c}^{P_{c}}$	n l j n	l' $l'$ $j'$	$E_{H}$	$J_{H}^{P_{H}}$	J	L	S	$[\mathrm{nb/sr}]$	
$0.000 \frac{11}{2}^{-}$	$0.5 \frac{11}{2} 0$	1 $\frac{3}{2}$	5.804	$7^+$	7	6	1	17.82	
$0.000 \frac{11}{2}^{-}$	$0 \ 5 \ \frac{11}{2} \ 0$	$1  \frac{1}{2}, \frac{3}{2}$	5.794	$6^+$	6	6	0,1	7.88	
$0.000 \frac{11}{2}^{-}$	$0.5 \frac{11}{2} 0$	$2 \frac{3}{2}, \frac{5}{2}$	11.875	$7^{-}$	7	7	0,1	18.02	
$0.000 \frac{11}{2}^{-}$	$0 \ 5 \ \frac{11}{2} \ 0$	$2 \frac{3}{2}, \frac{5}{2}$	11.934	$5^{-}$	5	5	0,1	0.20	
$0.000 \frac{11}{2}^{-}$	$0 \ 5 \ \frac{11}{2} \ 0$	$2 \frac{3}{2}, \frac{5}{2}$	11.946	$6^-$	6	5,7	1	1.27	
$0.000 \frac{11}{2}^{-}$	$0.5 \frac{11}{2} 0$	$2 \frac{5}{2}$	11.964	$8^{-}$	8	7	1	41.78	

phenomenological spectrum of <sup>207</sup> Tl									
core	proton	Λ	hypern	ucleus				cross sections	
$E_{c}  J_{c}^{P_{c}}$	$n \ l \ j \ n'$	l' $j'$	$E_{H}$	$J_{H}^{P_{H}}$	J	L	S	$[\mathrm{nb/sr}]$	
$1.348 \frac{11}{2}^-$	$0 \ 5 \ \frac{11}{2} \ 0$	$1 \frac{1}{2}, \frac{3}{2}$	6.974	$6^+$	6	6	0,1	7.44	
$1.348 \frac{11}{2}^-$	$0 \ 5 \ \frac{11}{2} \ 0$	$1 \frac{3}{2}$	6.984	$7^+$	7	6	1	16.62	
$1.348 \frac{11}{2}^-$	$0 \ 5 \ \frac{11}{2} \ 0$	$2 \frac{3}{2}, \frac{5}{2}$	13.109	$7^{-}$	7	7	0,1	10.65	
$1.348 \frac{11}{2}^-$	$0 \ 5 \ \frac{11}{2} \ 0$	$2 \frac{3}{2}, \frac{5}{2}$	13.110	$5^{-}$	5	5	0,1	0.63	
$1.348 \frac{11}{2}^-$	$0 \ 5 \ \frac{11}{2} \ 0$	$2 \frac{3}{2}, \frac{5}{2}$	13.122	$6^-$	6	5,7	1	1.37	
$1.348 \frac{11}{2}^-$	$0 \ 5 \ \frac{11}{2} \ 0$	$2 \frac{5}{2}$	13.144	8-	8	7	1	39.94	

TABLE III. The same as in Table II but for the  $\Lambda$  in the p(l'=1) and d(l'=2) orbit.

Predictions of excitation spectra in electroproduction of  $^{208}_{\Lambda}$ Tl are also compared with the previous result by Motoba nad Millener utilized in the proposal of the Jlab experiment E12-20-013 [8]. This older calculation was done for photoproduction at  $E_{\gamma}=1.5$  GeV and  $\theta_{K\gamma}=0.5^{\circ}$  using the Saclay-Lyon amplitude A (SLA) in the frosen-proton approximation ( $p_{eff}=0$ ). The  $\Lambda$  was assumed to be weakly coupled to the proton-

hole states of  $^{207}{\rm Tl}$ , which are strongly populated in the (e,e'p) and (d,  $^3{\rm He})$  reactions on  $^{208}{\rm Pb}$ , and the  $\Lambda$  single-particle energies were calculated from the Woods-Saxon potential. Our calculation for electroproduction was performed in the HF + TD $_{\Lambda}$  approach using the NN interaction D16+DDT with  $C_{\rho}=4000~{\rm MeV\cdot fm^6}$  and the SLA amplitude in the frosen-proton approximation assuming kinematics  $E_i=4~{\rm GeV},~E_f=2.5~{\rm GeV},$ 

 $\theta_e=2^\circ$ ,  $\theta_{Ke}=3.83^\circ$ , and  $\Phi_K=180^\circ$  giving photoproduction kinematics close to that by Motoba and Millener,  $E_\gamma=1.5~{\rm GeV}, |\vec{q}|=1.504~{\rm GeV/c}, Q^2=0.012~({\rm GeV/c})^2$ , and  $\theta_{K\gamma}=0.5^\circ$ . The relatively small value of  $Q^2$  allows a comparison with the photoproduction calculation.

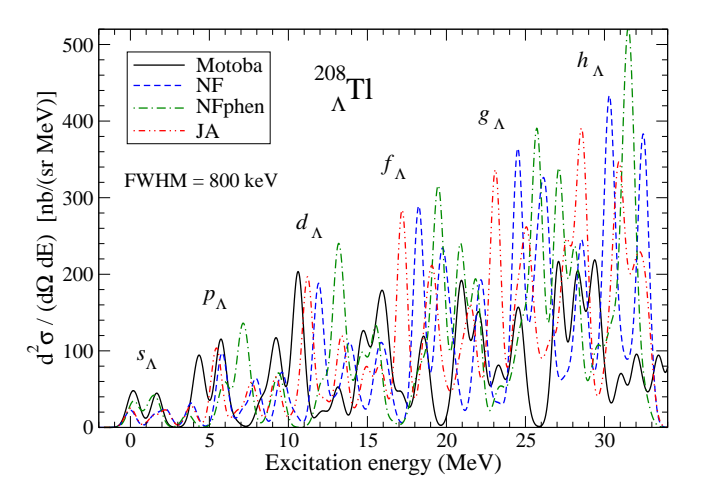


FIG. 13. Comparison of the result by Motoba and Millener [8] with our calculations in the HF + TD<sub> $\Lambda$ </sub> approach using the NN interaction D16+DDT with  $C_{\rho} = 4000 \text{ MeV} \cdot \text{fm}^6$  and the SLA amplitude in the frosen-proton approximation. The results were calculated with the Nijmegen F and Jülich A (JA) YNG interactions where the former was used with the original (NF) and phenomenological (NFphen) spectrum of  $^{207}$ Tl in Fig. 11. The curves are plotted with the width 800 keV for all states.

The results obtained with the Nijmegen F (NF) and Jülich A (JA) YNG interactions are compared with the result by Motoba and Millener in Fig. 13. In the case of Nijmegen YNG interaction we show both variants of the calculation, with the original (NF) and phenomenological (NFphen) spectrum of <sup>207</sup>Tl (see Fig. 11). One can see that in the new results the peaks with  $\Lambda$  in the d, f, g and h (for NFphen also p) orbits are shifted to larger values of the excitation energy with respect to Motoba-Millener's result where the shift is larger for the Nijmegen interaction. Moreover, the calculated cross sections for the high-laying states are systematically larger than the older values but they are a bit smaller for the  $s_{\Lambda}$  states. The best agreement is achieved with the NF and JA interactions for the second  $p_{\Lambda}$  peak composed mainly of the very close states  $(5.792 \text{ MeV}, 6^+), (5.804 \text{ MeV}, 7^+),$ and  $(5.831 \text{ MeV}, 5^+)$  with the NF and  $(5.425 \text{ MeV}, 7^+)$ ,  $(5.456 \text{ MeV}, 6^+)$ , and  $(5.463 \text{ MeV}, 5^+)$  with the JA interaction. These states are dominantly populated by the  $0h_{11/2} \to 0p_{3/2}$  and  $0h_{11/2} \to 0p_{1/2}$  transitions.

In the case of the  $s_{\Lambda}$  peaks in Fig. 13 the NFphen result agrees quite well with that by Motoba and Millener. This is because the phenomenological spectrum of  $^{207}$ Tl is consistent with the spectrum used by Motoba and Milenner [8]. Therefore, the left  $s_{\Lambda}$  peak is based

on the proton holes  $2s_{1/2}^{-1}$  and  $1d_{3/2}^{-1}$  and the right peak on  $1d_{5/2}^{-1}$  and  $0h_{11/2}^{-1}$  where contribution of the latter is negligible in the Motoba-Millener results but it is quite important in the NFphen result. On the contrary, in the NF and JA results the left peak is given by the  $0h_{11/2}^{-1}$  and  $2s_{1/2}^{-1}$  holes whereas the right one by the  $1d_{3/2}^{-1}$  hole.

Note that using the BS3 amplitude in the on-shell approximation changes mainly magnitudes of the main peaks at small excitation energies but at high energies the shape of the excitation spectrum is also changed which is due to the large density of hypernuclear states populated with different strength for the SLA and BS3 amplitudes.

One of the noticeable differences between our and Motoba-Millener's results is presence of a rising background in our result which causes that the peaks in the high-energy region of the spectrum are systematically rising. This phenomenon can be attributed to a high density of relatively weakly populated states in our calculations. In the JA calculation, there are about 630 states in the energy region 0-33 MeV, where most of the states are located above 10 MeV, and only 67 states are produced with the cross section larger than 5 nb/sr. On the other hand the older result includes only about 160 states. Note that in the Motoba-Millener's result presented in Ref. [8] the background is partially simulated assuming a larger width of the peaks above the quasi-free threshold but in the result presented here we plotted the spectrum with the uniform width 800 keV.

Finally, in Figure 14 we show predictions for the planned experiment E12-20-013 obtained with various forms of the effective YN interaction. The DWIA calculations for the Hall C kinematics [30] were performed in the HF + TD<sub> $\Lambda$ </sub> approach using the Daejeon 16 NN potential with the phenomenological DD term ( $C_{\rho} = 4000$ MeV·fm<sup>6</sup>) and the BS3 amplitude in the on-shell approximation. The results are for the YNG interactions Jülich A (JA), chiral in the leading order ( $\chi$ LO), and Nijmegen F. The latter was considered with the original (NF) and phenomenological (NFphen) spectrum of the core nucleus  $^{207}$ Tl. The G-matrix for the  $\chi$ LO potential was calculated with  $E_{\rm av} = -20.75$  MeV in Eqs. (6) and (7). The results in Fig. 14 show variety of predictions coming from different forms of the YNG interactions. A good quality experimental data, allowing determination of positions of the main peaks in the spectrum, could prefer one of the considered YNG interactions. Moreover, measured magnitudes of the peaks related to averaged cross sections can shed more light on dynamics of the process, the elementary amplitude and kaon distortion.

### V. SUMMARY AND CONCLUSIONS

We studied various effects in DWIA calculations of the cross sections in electroproduction of hypernuclei beyond the p shell. We analyzed the results in view of kaon distortion, kinematical effects, and various forms of

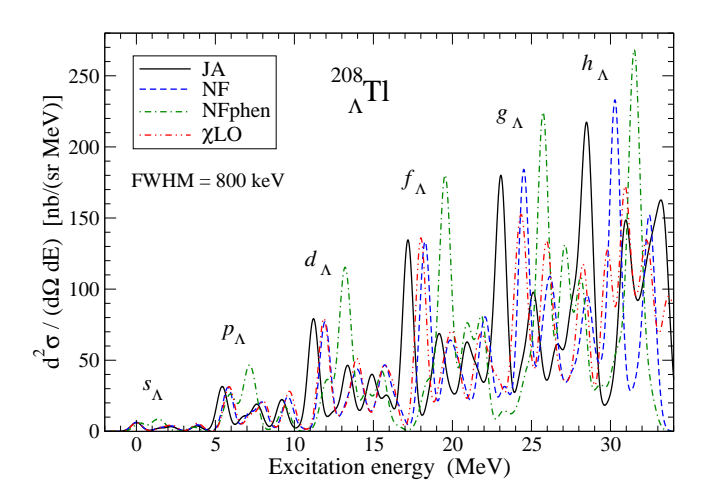


FIG. 14. Predicted spectrum of  $^{208}_{\Lambda}$ Tl in the Hall C kinematics of E12-20-013 calculated with the BS3 amplitude in the on-shell approximation for various forms of the baryon-baryon interaction: Jülich A (JA), Nijmegen F with original (NF) spectrum of  $^{207}$ Tl, Nijmegen F with phenomenological (NFphen) spectrum of  $^{207}$ Tl, and chiral leading order ( $\chi$ LO). For the G-matrix of the  $\chi$ LO potential, Eqs. (6) and (7) with  $E_{\rm av} = -20.75$  MeV were used.

the effective hyperon-nucleon interaction. The latter was aimed at illustrating uncertainties of predictions of the reaction cross sections due to variety of possible forms of the effective hyperon-nucleon interactions.

We showed that the damping effect of the kaon rescattering is rising with the hypernucleus mass, amounting 40–60% for  $^{40}_{\Lambda} \rm K$  and 50–80% for  $^{208}_{\Lambda} \rm Tl$  where the states with deeply bound  $\Lambda$  are more affected. The kaon distortion, accounted via the eikonal approximation with the first-order optical potential, depends mainly on behavior of the nucleon density in the peripheral region.

We have found that the momenta and the cross sections apparently depend on a tiny modification of the hypernucleus mass due to excitation energy, denoted as the hypernucleus-mass shift. This mass shift modifies the proton, kaon, and  $\Lambda$  momenta as well as the momentum transfer by a few per cents which changes values of the elementary amplitude and radial integrals. These changes then suppress the cross section by several per cents which is important mainly for the high-excited states.

We have elaborated our previously suggested optimum on-shell approximation [13] specifying yet free value of the angle  $\theta_{\Delta p}$ . In the new variant we suggest equate the magnitude of the proton effective momentum to a mean momentum of the proton in the single-particle or-

bit which corresponds to the dominant transition given by OBDME. The angle is then calculated from the energy conservation in the elementary vertex. This we denote as "on-shell approximation" where the elementary amplitude is on-shell with a specified non zero value of the proton momentum.

We demonstrated influence of various values of the proton effective momentum on the cross sections for electroproduction of  $^{208}$ Tl. In the given kinematics, differences between the proton- and  $\Lambda$ - frozen approximations amount up to 30% in the photon energy region 1.2–2.2 GeV. Similarly as for the p-shell hypernuclei [13] the effects are more apparent at small kaon angles. Influence of the selection rule [13], which controls contributions from the longitudinal mode of the virtual photon to the reduced amplitude, was also discussed for selected states of  $^{208}$ Tl.

We updated and discussed spectra in electroproduction of  $^{40}_{\Lambda}{\rm K}$  and  $^{48}_{\Lambda}{\rm K}$  using a new effective NN interaction, Daejeon 16 NN interaction complemented with the phenomenological DD term, and two forms of the YNG interaction, Nijmegen F and Jülich A. The results were calculated in kinematics of the planned experiment E12-15-008 at Jefferson Lab and they extend the discussion of predictions for the experiment initiated in Ref. [14]. We also discussed predictions for the electroproduction spectrum of  $^{52}_{\Lambda}{\rm V}$ . This spectrum clearly shows separated multiplets with  $\Lambda$  in the s,~p,~ and d orbits which might be suitable for an experimental investigation.

In the case of the  $^{208}{\rm Pb}$  target we discussed the results in view of various forms of the baryon-baryon interaction. We showed predictions with the Jülich A, Nijmegen F, and chiral leading-order YNG interactions and compared them with older calculations by Motoba and Millener utilized in preparing the experimental proposal E12-20-013 at Jefferson Lab. We also modified our calculations by using a phenomenological spectrum of the core nucleus  $^{207}{\rm Tl}$  and utilized this modified description in predicting the excitation spectra for  $^{208}_{\Lambda}{\rm Tl}$  in kinematics of the experiment E12-20-013. The results show that a good quality data could discriminate between various forms of the effective YNG interactions.

## ACKNOWLEDGEMENT

The work was supported by the Czech Science Foundation GACR, Grant No. P203-24-10180S. Computational resources were provided by the CESNET LM2015042 and the CERIT Scientific Cloud LM2015085, under the program "Projects of Large Research, Development, and Innovations Infrastructures".

A. Gal, E.V. Hungerford, and D.J. Millener, Rev. Mod. Phys. 88, 035004 (2016).

<sup>[2]</sup> O. Hashimoto and H. Tamura, Prog. Part. Nucl. Phys. 57, 564 (2006).

- [3] D. J. Millener, Nucl. Phys. A 804, 84 (2008); Nucl. Phys. A 881, 298 (2012).
- [4] P. H. Pile et al, Phys. Rev. Lett 66, 2585 (1991).
- [5] T. Miyoshi et al, Phys. Rev. Lett 90, 232502 (2003).
- [6] F. Garibaldi et al, Phys. Rev. C 99, 054309 (2019).
- [7] F. Garibaldi, P.E.C. Markowitz, S.N. Nakamura, J. Reinhold, L. Tang, and G.M. Urciuoli (spokespersons), JLab experiment E12-15-008, An isospin dependence study of the ΛN interaction through the high precision spectroscopy of Λ-hypernuclei with electron beam, https://www.jlab.org/exp\_prog/proposals/16/C12-15-008.pdf.
- [8] O. Benhar, F. Garibaldi, P.E.C. Markowitz. Nakamura, J. Reinhold, L. Tang, S.N. Urciuoli (spokespersons), JLab experiment Studying  $\Lambda$  interactions the  $^{208}{\rm Pb}({\rm e,e'K^+})^{208}_{\Lambda}{\rm Tl}$ E12-20-013, in nuclear with reaction, https://www.jlab.org/exp\_prog/proposals/20prop.html.
- [9] T. Motoba, P. Bydžovský, M. Sotona, and K. Itonaga, Prog. Theor. Phys. Suppl. 185, 224 (2010).
- [10] P. Bydžovský, M. Sotona, T. Motoba, K. Itonaga, K. Ogawa, and O. Hashimoto, Nucl. Phys. A 881, 199 (2012).
- [11] T. Motoba, JPS Conf. Proc. 17, 011003 (2017).
- [12] P. Bydžovský, D.J. Millener, F. Garibaldi, and G.M. Urciuoli, AIP Conf. Proc. 2130, 020014 (2019).
- [13] P. Bydžovský, D. Denisova, D. Skoupil, and P. Veselý, Phys. Rev. C 106, 044609 (2022).
- [14] P. Bydžovský, D. Denisova, D. Petrellis, D. Skoupil, P. Veselý, G. De Gregorio, F. Knapp, and N. Lo Iudice, Phys. Rev. C 108, 024615 (2023).
- [15] D. Denisova, PhD Thesis, Electroproduction of Hypernuclei, Institute of Particle and Nuclear Physics, Charles University, Prague, 2024, https://dspace.cuni.cz/bitstream/handle/20.500.11956/ 195141/140122373.pdf.
- [16] J. Pokorný, G. De Gregorio, F. Knapp, N. Lo Iudice, and P. Veselý, Phys. Pol. B Proc. Suppl. 12, 657 (2019).
- [17] D. Bianco, F. Knapp, N. Lo Iudice, P. Veselý, F. Andreozzi, G. De Gregorio, and A. Porrino, J. Phys. G: Nucl. Part. Phys. 41, 025109 (2014).

- [18] A. Shirokov, I. Shin, Y. Kim, M. Sosonkina, P. Maris, and J. Vary, Phys. Lett. B 761, 87 (2016).
- [19] Daejeon16 NN Interaction Software, https://dr.lib.iastate.edu/handle/20.500.12876/23380
- [20] D. R. Entem and R. Machleidt, Phys. Rev. C 68, 041001(R) (2003).
- [21] F. Wegner, Ann. Phys. 506, 77 (1994).
- [22] Y. Yamamoto, T. Motoba, H. Himeno, K. Ikeda, and S. Nagata, Prog. Theor. Phys. Suppl. 117, 361 (1994).
- [23] H. Polinder, J. Haidenbauer, and U.-G. Meißner, Nucl. Phys. A 779, 244 (2006).
- [24] P. Bydžovský and M. Sotona, Separable model for K<sup>+</sup>-nucleon scattering, in Proc. 7th Conference on Mesons and Light Nuclei, Praha-Průhonice, Czech Republic, 31 Aug. 4. Sept., 1998. Eds. J. Adam, P. Bydžovský, J. Dobeš, R. Mach, J. Mareš, and M. Sotona (World Scientific, Singapore, 1999), p. 138.
- [25] P. Bydžovský and M. Sotona, Elastic Scattering of K<sup>+</sup> from Light Nuclei, in Proc. 6th Conference on Mesons and Light Nuclei, Eds. J. Adam, J. Dobeš, R. Mach, M. Sotona, and J. Dolejší, Few-Body Systems Suppl. 9, 61 (1995).
- [26] P. Bydžovský and M. Sotona, Czechoslovak Journal of Physics, 48, 903 (1998).
- [27] B. R. Martin, Nucl. Phys. B **94**, 413 (1975).
- [28] D. Skoupil, P. Bydžovský, Phys. Rev. C 93, 025204 (2016); ibid. 97, 025202 (2018).
- [29] A. Ekström, G. R. Jansen, K. A. Wendt, G. Hagen, T. Papenbrock, B. D. Carlsson, C. Forssén, M. Hjorth-Jensen, P. Navrátil, and W. Nazarewicz, Phys. Rev. C 91, 051301(R) (2015).
- [30] Private communication by S.N. Nakamura: Kinematics of the experiment E12-20-013 was changed with respect to that in Hall A [8]. The new kinematics in Hall C is  $E_i = 2.24 \text{ GeV}, E_f = 0.74 \text{ GeV}, \theta_e = 8^{\circ}, \theta_{Ke} = 11^{\circ}, \text{ and } \Phi_K = 180^{\circ}.$
- [31] E. Wilson et al, Phys. Lett. B 747, 88 (2015).
- [32] F.G. Kondev and S. Lalkovski, Nuclear Data Sheets 112, 707 (2011).
- [33] Peter K.A. de Witt Huberts, Nucl. Phys. A 507, 189c (1990).

